Progress In Electromagnetics Research B, Vol. 45, 269–290, 2012

A NEW APPROACH TO ANALYSIS OF INDUCTION MOTORS WITH ROTOR FAULTS DURING STARTUP BASED ON THE FINITE ELEMENT METHOD

V. V. Kuptsov*, A. S. Sarvarov, and M. Y. Petushkov

Magnitogorsk State Technical University, 38 Lenin St., Magnitogorsk 455000, Russia

Abstract—The increasing popularity of a so-called transient motor current signature analysis requires the fault diagnostics parameters which could not be exposed to other factors irrelevant to the fault to make a precise assessment of the failure severity level. This challenging task needs a precise modeling of faulty motor behavior in various operating conditions at different fault severity levels. This paper introduces a new approach to the finite element analysis of an induction motor with broken rotor bars during startup. The approach is based on the principle of superposition and contributes to examination of the fault rotor backward rotating magnetic field and current components produced by such field separating them from stator currents. It gives a new sight on the behavior of a faulty motor during startup for the diagnosis purposes. Further analysis of the simulation data by means of the Extended Park's Vector Approach and the continuous wavelet transform and its experimental validation is also presented in the paper.

1. INTRODUCTION

Nowadays squirrel-cage induction motors are widely used in many industrial applications thanks to their usability, robustness as well as low maintenance costs. However, in spite of their reliability, they are eventually subjected to deterioration that can lead to a motor failure. Unscheduled equipment downtime can often cause significant financial losses. Early fault detection and preventive maintenance contribute to prediction of stoppages caused by an unexpected motor failure, improving the overall reliability of the motor driven system.

Received 29 August 2012, Accepted 29 October 2012, Scheduled 31 October 2012

* Corresponding author: Vladimir Kuptsov (2v.kuptsov@gmail.com).

The motor current signature analysis (MCSA) is a traditional technique for detection of broken rotor bars in induction motors [1–6]. MCSA is mainly based on the study of the stator currents in steady-state using the Fast Fourier transform (FFT) and currently well recognized as a standard. Bar breakages in the induction machine cause some additional current components in the stator windings. The most relevant ones are well known as left and right sideband harmonics and their frequencies are given by (1) [4–6].

$$f_{SB} = f_1(1 \pm 2s) \tag{1}$$

where s is the machine slip, f_1 is the fundamental supply frequency.

However, FFT can provide inaccurate results when the speed or the load torque is not constant, making it not suitable for motors, operating predominately in transient conditions. Moreover, applying techniques in a steady state it is difficult to detect broken rotor bars in low-load operating conditions.

In order to overcome these drawbacks and expand the application of MCSA, some new methods, based on the examination of the induction motor startup, have been proposed [7–16]. During startup the motor slip varies within a wide range that allows detecting additional current components caused by broken bars more easily. Furthermore, the motor in startup conditions is exposed to dynamic loads. Thus, in these cases such methods can provide an accurate diagnosis irrespective of the motor loads.

In order to increase the accuracy of approaches based on the transient analysis, a thorough understanding of the effect of the broken bars on the stator currents in a machine is crucial. In the case of a broken bar, the induction machine behavior can be understood using the principle of superposition and superimposed fault currents introduced by Deleroi [17]. According to this approach the faulty machine can be examined as the superposition of two configurations: the machine in a healthy state plus the machine with a current source placed in a broken bar and injecting a current of opposite value as the current flowing in the same bar of the healthy machine. The resulting current in the broken bar is therefore zero. The current source of the second configuration produces a magnetic field inducing the additional current harmonics in the stator windings that are used for the bar breakage diagnosis. Based on this fact, a method for approximate calculation of the evolution of the left sideband harmonic during the startup in a cage motor with a broken bar has been proposed in [18]. However, the method disregards the saturation of the iron core and skin effect in rotor slots essential to the startup transient. Therefore, its accuracy is too low for the deep interpretation of the physical phenomenon related to the rotor faults in induction motors. Another

study in [19] presents the finite element analysis and validation of the principle of superposition in the case of a linear machine (i.e., iron has constant permeability) and in the case of a machine with local saturation. But the mentioned study deals only with a steady state and the transient regimes have not been considered.

The modeling of squirrel cage induction motors with broken rotor bars is widely studied in the literature [19–26]. Among these methods the time-stepping finite element (TSFE) modeling is considered as the most precise way since it is based on a very close geometry of the machine and the real nature of the electromagnetic phenomenon taking place in an induction motor [19, 23–27].

This paper presents a new approach to precise assessment of the effect of the broken rotor bars on the stator currents in an induction machine during startup through direct calculation of the current harmonics caused by the rotor failure. One of the main novelties of this approach is the use of the time-stepping finite element method to increase accuracy of the calculation together with the superposition principle. Modifications presented herein and applied to the Deleroi superposition principle to take into consideration the saturation of the iron core and skin effect in rotor slots have never been published either; these modifications allow using the superposition principle, which is in general valid only for linear systems, for nonlinear simulation. Another contribution of this paper is the validation of the modified principle of superposition for startup taking into account saturation and skin effect.

In this paper, the FEM model is used for analysis of a faulty induction motor. The proposed approach is used to study the influence of the broken rotor bars on an induction motor startup at no load. The simulation data is analyzed by means of the Extended Park's Vector Approach and the continuous wavelet transform. Study results are discussed and compared with similar, previously introduced ones. Finally, the validation of the proposed approach with the experimental results is given herein.

2. INDUCTION MACHINE FE SIMULATION

In this study, the TSFE method is used to investigate the influence of the broken rotor bars on the stator currents during direct on-line startup of the induction motor. The TSFE model has been developed in Matlab programming language and takes into account the geometry of the cross-section of the machine including a number and a shape of stator and rotor slots, both space and time harmonics of the instantaneous magnetic field inside the machine, nonlinear characteristics of the cores, resistance of rotor bars and end-rings, skin

effect in rotor slots.

The model is based on Maxwell's equations with an assumption that the magnetic field does not depend on z-coordinate being parallel to the axis of rotor shaft. Then the magnetic field calculation problem is solved by using a 2D Finite Element Method. The electric circuits (the stator and rotor windings) are coupled with the magnetic field by means of a technique proposed by the authors [25]. This technique allows calculating the current flowing in each mesh element of a rotor slot and therefore to take into account the uneven current distribution over the cross-section of a rotor slot caused by influence of the skin effect during startup. The electromagnetic torque is computed by integrating the Maxwell stress tensor.

This section describes two FE simulations conducted for two cases of a startup transient. The machine used in the simulation is a three-phase induction motor (380 V, 0.5 kW, with 4 poles) supplied with a sinusoidal voltage, 50 Hz, and started at no load. The same motor type has been used throughout the study.

The two FE simulations are:

HealthyMotorSim: represents the motor in a healthy condition.

FaultyMotorSim: represents the motor with two broken rotor bars.

Bars intended to be broken are simulated by assuming that their conductance is zero. Inter-bar currents are disregarded. The mesh used for FE modeling is shown in Fig. 1 and has 19 360 elements and 9753 nodes, the time step Δt is 0.0001 seconds. At each time step of the simulation process the permeability of each iron element of the faulty model is stored in files. These files will be used in further simulations explained in the next section.

Figure 2 shows the starting current of phase A for both cases. It is clearly seen that differences between healthy and faulty motors are faintly visible in the transient currents and would not be favorable for the detection of broken bars. Nevertheless, as shown in Figs. 3 and 4, the instantaneous magnetic flux distribution (at the instant of 0.024 s) around the broken bars undergoes significant changes. The bar breakage leads to redistribution of its current to adjacent bars resulting in local perturbation of the magnetic flux distribution. The study in the following section is focused on influence of this asymmetrical magnetic field produced by a rotor failure on starting currents using the principle of superposition.

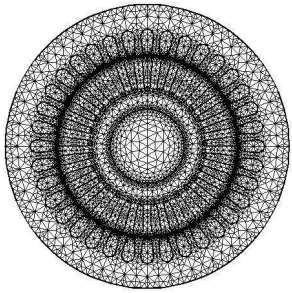

Figure 1. The finite elements mesh of the machine.

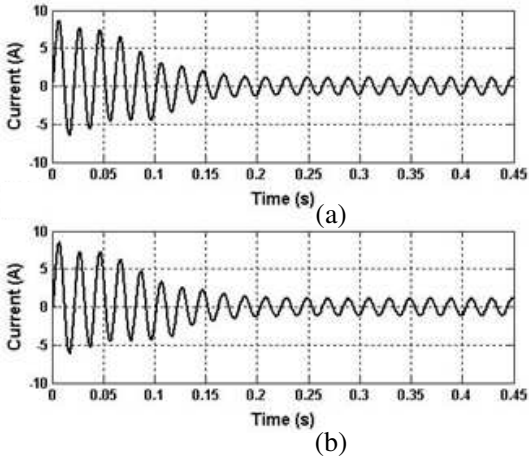

Figure 2. The simulated starting current (phase A) of (a) a healthy motor and (b) a faulty motor with 2 broken bars started at no load.

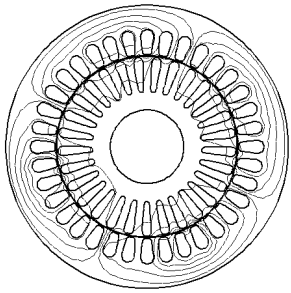

Figure 3. The instantaneous magnetic flux distribution of a healthy motor at the instant of 0.024 s.

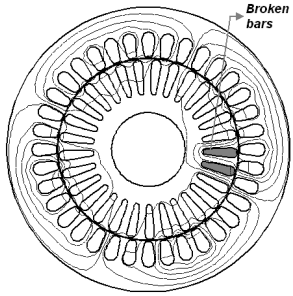

Figure 4. The instantaneous magnetic flux distribution of a faulty motor with 2 broken rotor bars at the instant of 0.024 s.

3. COMBINATION OF FE SIMULATION AND THE PRINCIPLE OF SUPPOSITION: APPROACH TO THE FAULT CURRENT HARMONICS CALCULATION

First, let us consider the induction machine behavior under steady-state operation and in a healthy condition. The three-phase currents in the stator windings create a forward rotating field with speed ω. The rotor rotates at a speed of $(1-s)\omega$ and therefore the stator magnetic field rotates at $s\omega$ with respect to the rotor. Stator field induces currents in rotor bars which create a rotor magnetic field rotating at $s\omega$ in the forward direction with respect to the rotor. The rotor field therefore rotates at speed ω with respect to the stator and does not induce new current components in the stator windings.

As it was previously pointed out, the behavior of an induction machine with a broken rotor bar can be understood using the Deleroi principle of superposition. The current source placed in a broken bar produces an additional rotor magnetic field rotating at $s\omega$ in the backward direction with respect to the rotor. This rotor backward rotating field rotates at speed:

$$\omega_{rbw} = (1-2s)\omega \tag{2}$$

with respect to the stator and induces currents at frequency $(1-2s)f_1$ in the stator windings, which is the left sideband harmonic in (1). Speed and torque oscillations occur at $2sf_1$ and this induces the right broken bar sideband harmonic.

The main idea of modifications used to apply the Deleroi superimposed approach for startup can be explained using two additional FE simulations *SuperposPrincSim1* and *SuperposPrincSim2* carried out in this study. These simulations correspond to two configurations whose sum according to the superposition principle represents the faulty machine from *FaultyMotorSim*. The purpose of

this part of the study is to estimate fault current harmonics in stator windings caused by two broken bars separating them from starting currents and to examine their behavior during startup. Statements for *SuperposPrincSim1* and *SuperposPrincSim2* are given below:

3.1. SuperposPrincSim1

The machine used in this simulation is an induction motor identical to one used in the study of the previous section with no broken bars supplied with three-phase sinusoidal voltage. The rotor position of the machine at each time step of the simulation process is assumed to coincide with the rotor position computed by *FaultyMotorSim* for the same instant of simulation time. In order to take into account the local saturation of the iron core around bars intended to be broken in the faulty motor, the above-mentioned files saved by *FaultyMotorSim* are used. The permeability of each mesh element of the iron core in *SuperposPrincSim1* is determined to be equal to the value computed by the faulty FE model and loaded from the appropriate file for the same working point. It means that the simulation *SuperposPrincSim1* represents a healthy machine in which, at each simulation time step, the permeability of the iron core and rotor speed remain equal to the faulty situation *FaultyMotorSim*. At each time step of the simulation process the current density of each rotor bar element of the *SuperposPrincSim1* model is stored in files in order to be used in *SuperposPrincSim2*.

3.2. SuperposPrincSim2

Herein the machine is running with short-circuited stator windings and current sources placed in each broken bar. As mentioned above, the current distribution over the cross-section of a rotor slot is uneven and the model calculates the current flowing in each mesh element of considered slot instead of the total current of the bar. The broken bar current source therefore should be replaced by several sources in parallel each of them injecting a current in its mesh element with a value computed by *SuperposPrincSim1* and loaded from the appropriate file but opposite in direction. The summarized current obtained by adding the *SuperposPrincSim1* and *SuperposPrincSim2* configurations for each broken bar is therefore zero. The permeability of the iron and rotor speed at each simulation time step also remains equal to the faulty situation *FaultyMotorSim* as in previous simulation. The rotor magnetic field created by the faulty current sources induces currents in stator windings which according to

the principle of superposition can be considered as broken rotor bar additional components of starting stator currents.

3.3. Validation

For validation of the principle of superposition for startup the stator currents of phase A based on results of two simulations *SuperposPrincSim1* and *SuperposPrincSim2* are added and compared to the current of the faulty machine computed by *FaultyMotorSim*. An error $\varepsilon(t)$ is defined as:

$$\varepsilon(t) = abs[Ia_{Sup1}(t) + Ia_{Sup2}(t) - Ia_{Faulty}(t)]/RMS(Ia_{Faulty}(t))$$

The error $\varepsilon(t)$ calculated in this way for each time step is lower than 0.2% with its mean value lower than 0.05% and determined only by a residual error of the nonlinear solver algorithm.

The simulation results represented as curves of fault related current components estimated by *SuperposPrincSim2* are shown in

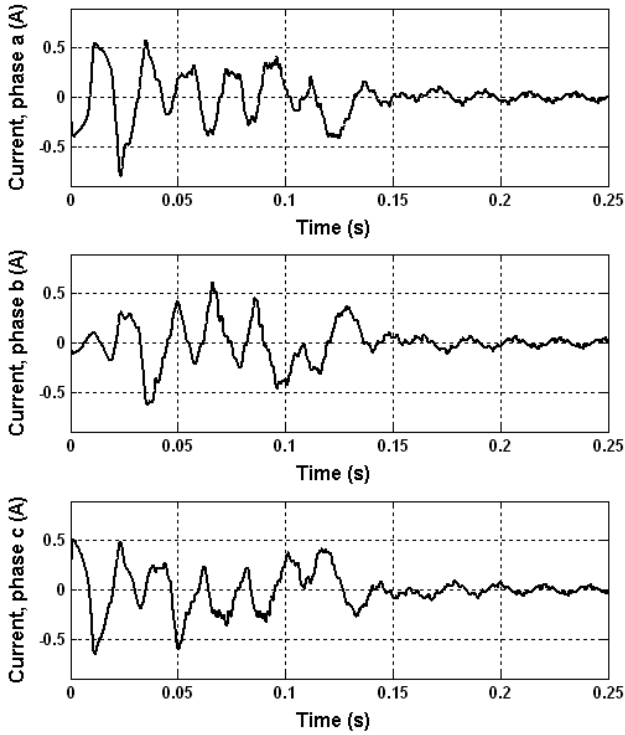

Figure 5. The rotor fault additional current components estimated by FE simulation and the principle of superposition.

Fig. 5. Their theoretical and experimental validation is given in the following sections. The proposed approach can facilitate the deep interpretation of the physical phenomenon related to the rotor faults in induction motors in various operating conditions and at different fault severity levels.

4. BROKEN ROTOR BARS FAULT STUDY

The aim of this section is a thorough analysis of the simulation data obtained in previous sections through their theoretical interpretation, discussion and comparison with previously introduced results. In order to analyze the data in frequency and time domains, the continuous wavelet transform is chosen. To eliminate the stator current fundamental frequency component from a signal, the data preprocessing using Extended Park's Vector Approach is proposed.

4.1. The Extended Park's Vector Approach

Figure 6 depicts the comparison between the starting current of phase A of the faulty machine from *FaultyMotorSim* and estimated rotor failure current components from *SuperposPrincSim2*. As it can be observed the amplitude of additional components is much less than the amplitude of the fundamental supply frequency component that makes it difficult to distinguish between a healthy motor and a faulty one with broken rotor bars. The problem of masking of the fault signatures by a strong fundamental component is widely studied in the literature. As a solution, in [11] an adaptive notch filter and in [28] a bandpass filter are applied to remove the fundamental frequency from the stator current. In [15] a discrete wavelet transform (DWT) is used to extract the left sideband harmonic from the starting current.

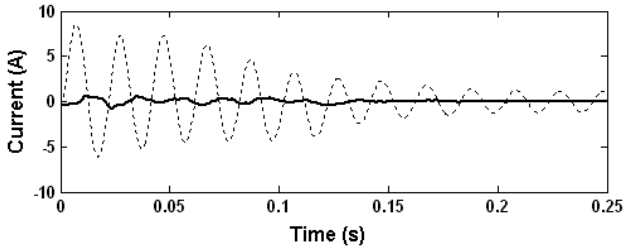

Figure 6. The starting current of a faulty motor with 2 broken bars (dotted) and estimated rotor fault additional current components (solid).

The other method in [16] involves an envelope extraction technique. An interesting method based on the reference frame theory approach is proposed in [29]. However, the approach used in [29] requires a precise speed measurement and cannot be applied for speed sensorless drive systems. Filtering out of the fundamental component in the stator current cannot be used either, since it can affect additional current components and thus can lead to incorrect results. Another approach that does not affect additional components or require speed measurement has been used in the following sections. This approach is based on examination of the Park's vector magnitude and known as the Extended Park's Vector Approach (EPVA) [30].

Park's transformation is used to transform instantaneous stator currents from the three-phase system (a-b-c) to the two-phase system (d-q). The expressions for the transformation are:

$$\begin{aligned} I_d &= i_a - \frac{1}{2} i_b - \frac{1}{2} i_c \\ I_q &= \frac{\sqrt{3}}{2} i_b - \frac{\sqrt{3}}{2} i_c \end{aligned} \tag{3}$$

The expression for the Park's vector magnitude (PVM) is

$$I_S = \sqrt{I_d^2 + I_q^2} \tag{4}$$

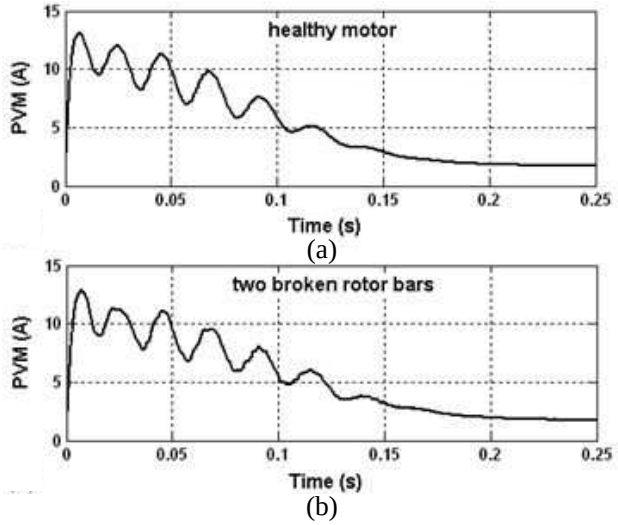

Figure 7. The PVM of the simulated startup transient of (a) a healthy motor and (b) a faulty motor with two broken rotor bars.

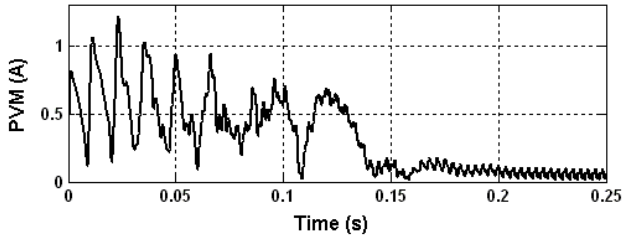

Figure 8. The PVM of rotor fault additional current components.

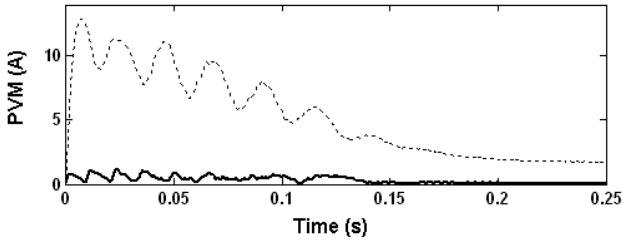

Figure 9. The PVM of a faulty motor with 2 broken bars during startup (dotted) and the PVM of rotor fault additional current components (solid).

Thus, the EPVA converts three-phase stator current to equivalent DC value, which can be easily filtered out from the original signal and additional components can therefore show up more clearly.

Figure 7 shows the PVM of FE simulated startup transient for the cases of healthy and faulty motors. As one can notice, the waveform of the faulty motor curve is slightly distorted due to additional current components caused by two broken bars. It shows that after applying the EPVA to starting currents the fundamental 50 Hz component has been successfully removed revealing the changes in the current waveform caused by the asymmetrical magnetic field shown in Fig. 4.

Current components shown in Fig. 5 have been transformed using (3) and (4) and the resulting curve is depicted in Fig. 8. The comparison between starting currents of the faulty machine and estimated rotor failure current components after applying the EPVA is shown in Fig. 9. Comparing Figs. 6 and 9 and taking into account that the DC component of the PVM of the supply current can be easily eliminated the advantage of this approach for broken bars detection is quite evident though it requires the measurement of at least two stator currents (the third is obtained as a sum of the first two).

4.2. Wavelet Analysis and Broken Rotor Bars Detection Patterns

It can be shown that the rotor fault components determined by (1) appear in the PVM at the frequency:

$$f_{SB}^{PVM} = 2sf_1 \tag{5}$$

According to (5) at the beginning of the startup the frequency of these components is maximum and equals to 100 Hz. As the slip changes during startup the frequency decreases and becomes almost zero in a steady state. The corresponding frequency evolution is shown in Fig. 10(a).

The startup transient is a non-stationary process. One of the most powerful tools for a non-stationary or time varying signal analysis is

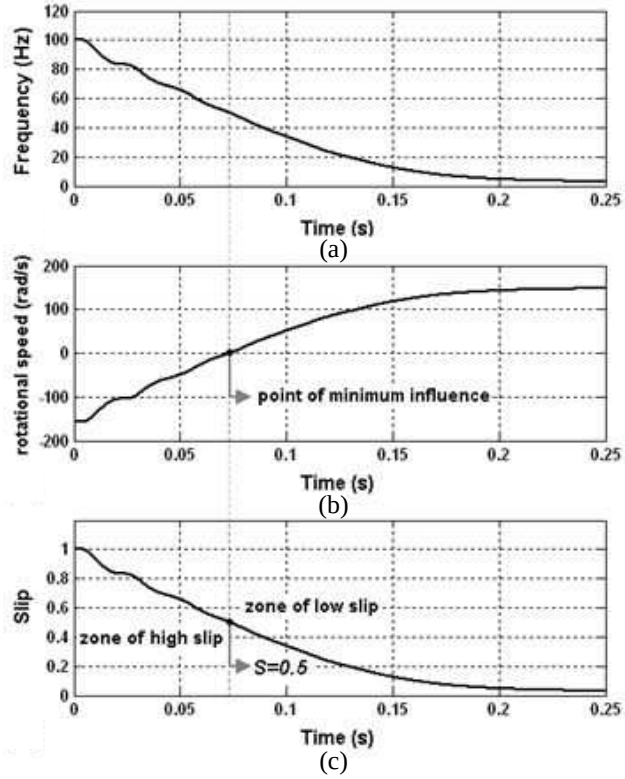

Figure 10. (a) The theoretical frequency evolution of the PVM of the left and right sideband harmonics. (b) Speed of the backward rotating rotor magnetic field. (c) The machine slip.

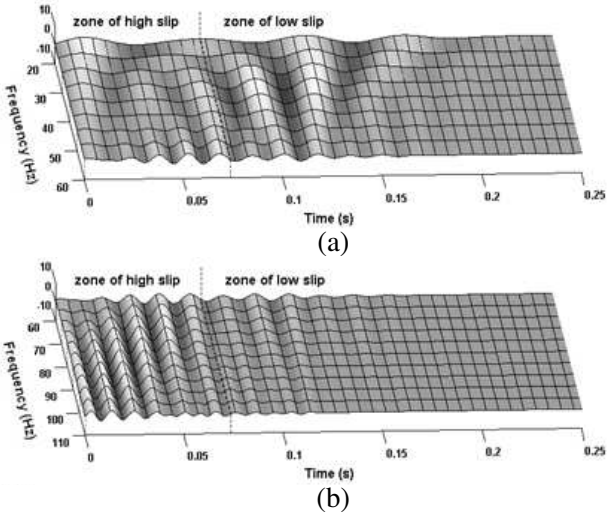

Figure 11. The CWT spectrograms of the PVM of the simulated fault additional components for the frequency range (a) from 20 to 60 Hz and (b) from 60 Hz to 110 Hz.

a Wavelet Transform [31–33], providing some advantages if compared to other signal processing methods like Fourier Transform and Short-Time Fourier Transform. In the last few years several authors have focused their efforts on the applying this tool for the diagnosis of broken rotor bars. The applying of DWT has been widely discussed for current analysis during startup [8, 10, 11, 14], under speed and load torque variations [34–36] and during plugging stopping [10]. A contribution based on wavelet ridge was presented in [13]. In [16] the continuous wavelet transform (CWT) is used for the envelope analysis of the starting current. The Wavelet Transform can be considered as filtering out a signal with several bandpass filters while each of them extracting the components within the particular frequency range and thus representing the signal in both time and frequency domains.

As it was previously pointed out, the bar breakage produces rotor backward rotating field. According to (2) at the time point when the value of the machine slip decreases to 0.5, the backward rotating field changes its direction with respect to the stator. As at this time the speed of the rotating field equals to zero, the rotor failure therefore exerts a minimum influence on the stator currents (Fig. 10(b)). Further analysis shows that the change of the direction of the field rotation also causes the change of the behavior pattern of the additional current components induced by that field. In this connection it is suggested

that the startup should be divided into two zones in the time domain (Fig. 10(c)). First zone, hereinafter a zone of high slip, corresponds to the machine slip range from 1 to 0.5. Second zone, hereinafter a zone of low slip, has the slip range from 0.5 to the steady state value.

Figure 11 shows spectrograms of the PVM of the rotor fault components obtained by the CWT, demonstrating different behavior patterns in the frequency domain for different machine slip ranges. It can be observed that these patterns correspond to the theoretical frequency evolution of $2sf_1$ component in the starting PVM signal displayed in Fig. 10(a) which proves that the left and right sideband harmonics prevail over the other fault components in the specified frequency range. Regarding the amplitude pattern, as it was expected, the wavelet coefficient values decrease when the rotor fault magnetic field changes its direction, i.e., when the slip equals to 0.5. The frequency and amplitude patterns presented in Fig. 11 also agree with issues previously reported in [7, 10, 14, 15, 18].

The more wavelet coefficient values in the specified time and frequency range, the more power carried by fault components is concentrated in such range and ultimately it is more clearly that they

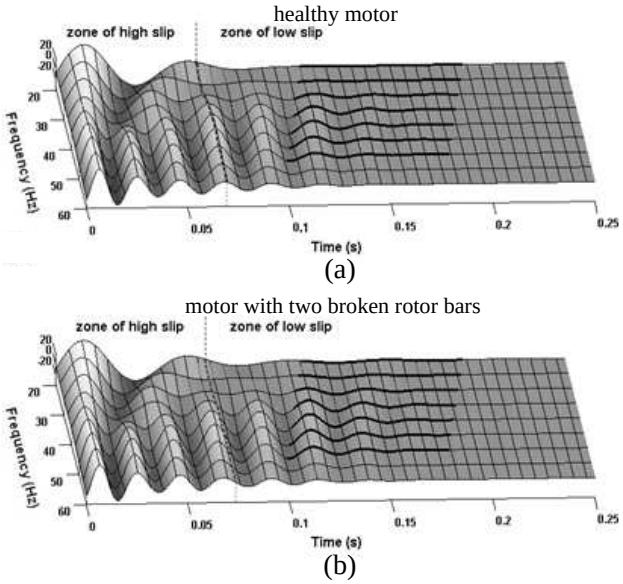

Figure 12. The CWT spectrograms of the simulated PVM of (a) a healthy motor and (b) a faulty motor with 2 broken rotor bars during startup (frequency range: 20–60 Hz).

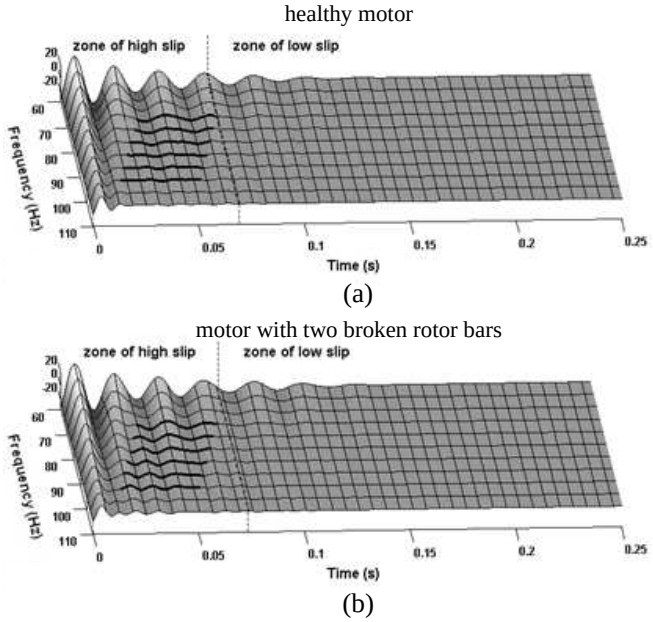

Figure 13. The CWT spectrograms of the simulated PVM of (a) a healthy motor and (b) a faulty motor with 2 broken rotor bars during startup (frequency range: 60–110 Hz).

appear in the PVM signal. Figs. 12 and 13 depict wavelet spectrograms of PVM signals shown in Fig. 7. These figures demonstrate how the characteristic patterns introduced by fault components influence the spectrogram waveform of the motor with two broken bars. Comparing these spectrograms, it can be noticed that though in the zone of low slip the differences are not significant, they are quite evident in the zone of high slip. The presence of two broken rotor bars in the machine and, therefore, occurrence of the fault components in the stator current increase the ripple of wavelet coefficients in the selected area of the zone of high slip that can be used for detection of the fault.

A practical remark should be made. The CWT is preferred in this study only to facilitate the understanding of the examined phenomenon since it provides more flexible analysis comparing to DWT. On the other hand, the CWT requires higher computing power as compared to DWT because information provided by the CWT is highly redundant. Therefore, for industrial applications the DWT will be a more reasonable choice.

5. EXPERIMENTAL RESULTS

In order to validate the simulation results several experiments have been performed. The motor used in experiments is identical to the simulated one (4 poles, 29 rotor bars, 380 V, 0.5 kW, 50 Hz) and tested in the same conditions. Two line currents are captured using a PC-based data acquisition system with a sampling frequency of 8 kHz. The motor is started at no load in healthy conditions and with a faulty rotor that has two and four broken bars. The bars are broken by drilling a hole in them. Fig. 14 shows the experimentally measured PVM signals of the healthy motor and the motor with two and four broken bars during a startup transient. The obtained data has been processed using the CWT of the Matlab Wavelet Toolbox. The resulting wavelet spectrograms are given in Figs. 15 and 16. As it follows from figures, these spectrograms show the behavior patterns

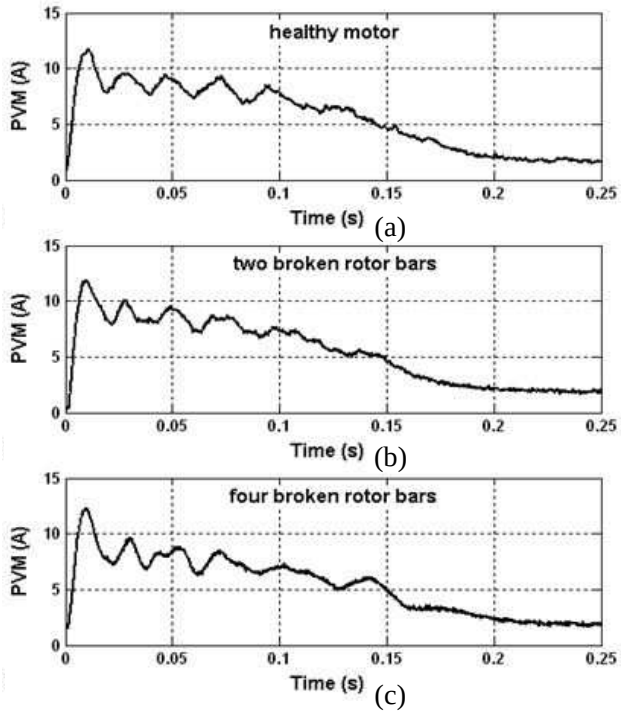

Figure 14. The experimentally measured PVM of (a) a healthy motor, (b) a faulty motor with 2 broken rotor bars and (c) a faulty motor with 4 broken rotor bars during startup.

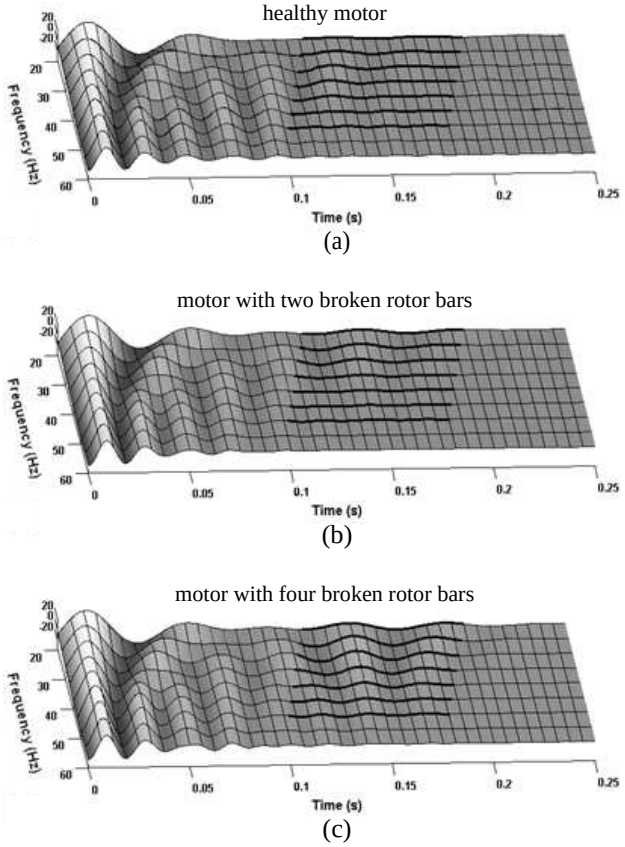

Figure 15. The CWT spectrograms of the experimentally measured PVM of (a) a healthy motor, (b) a faulty motor with 2 broken rotor bars and (c) a faulty motor with 4 broken rotor bars during startup (frequency range: 20–60 Hz).

similar to those displayed in Figs. 12 and 13 for simulated results. The healthy motor (Figs. 15(a) and 16(a)) shows some initial ripple of the wavelet coefficients of the selected areas in both high and low slip zones due to the intrinsic rotor asymmetry. As it was predicted by the modeling in previous sections, the breakage of two bars (Figs. 15(b) and 16(b)) increases the ripple of wavelet coefficients in the zone of high slip and slightly influences the spectrogram waveform in the zone of low slip. Moreover, the drilling of two additional bars (Figs. 15(c) and 16(c)) leads to subsequent increase in the ripple of wavelet coefficients not only in the high slip zone but also in the zone of low slip.

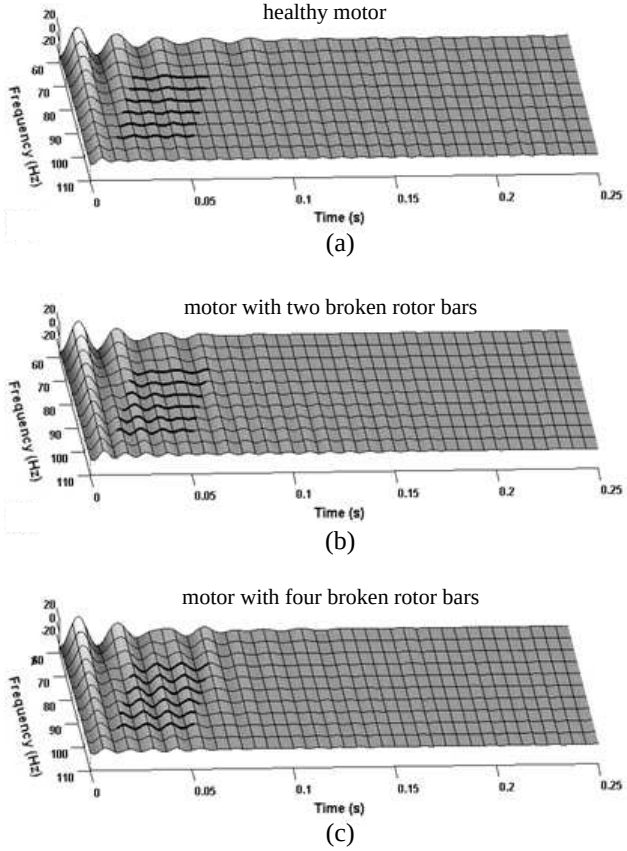

Figure 16. The CWT spectrograms of the experimentally measured PVM of (a) a healthy motor, (b) a faulty motor with 2 broken rotor bars and (c) a faulty motor with 4 broken rotor bars during startup (frequency range: 60–110 Hz).

6. CONCLUSIONS

This paper presents a new approach to precise assessment of the effect of the broken rotor bars on the stator currents in an induction machine during startup providing a deep understanding of the fault related phenomenon for diagnostic purposes. The principle of superposition explaining behavior of a faulty rotor induction machine in a steady-state has been extended and applied for the startup. It is shown that the combination of the superposition principle with the time-stepping finite element method provides accurately estimated stator current

components caused by the rotor failure. It can be used to establish the fault severity quantification parameters independently of motor operating conditions, a chosen signal processing tool and other factors not related to the rotor failure, which are considered as future work in this study. The validation of the proposed approach shows a good agreement with the experimental results as well as with the issues previously reported in the technical literature.

The method combining the wavelet transform with the Extended Park's Vector Approach has been used for analysis of the simulated and experimental data. It is shown that the Extended Park's Vector Approach allows improving the sensitivity of the wavelet transform for rotor faults detection comparing to methods involving only one line current as input due to its inherent ability to eliminate the stator current fundamental frequency component. However, its implementation requires a measurement of one additional line current and the choice of the single-current or two-current diagnostic approach is a matter of a reasonable balance between the cost and reliability of the diagnostic system.

REFERENCES

1. Thomson, W. T. and M. Fenger, "Current signature analysis to detect induction motor faults," *IEEE Industry Applications Magazine*, Vol. 7, No. 4, 26–34, Jul./Aug. 2001.
2. Kliman, G. B. and J. Stein, "Induction motor fault detection via passive current monitoring," *Proc. of Int. Conf. Electrical Machines, (ICEM)*, 13–17, 1990.
3. Nandi, S. and H. A. Toliyat, "Condition monitoring and fault diagnosis of electrical machines — A review," *Proc. of Industry Applications Conference*, Vol. 1, 197–204, 1999.
4. Kliman, G. B., R. A. Koegl, J. Stein, R. D. Endicott, and M. W. Madden, "Noninvasive detection of broken rotor bars in operating induction motors," *IEEE Trans. Energy Convers.*, Vol. 3, No. 4, 873–879, Dec. 1998.
5. Elkasabgy, N. M., A. R. Eastham, and G. E. Dawson, "Detection of broken rotor bars in the cage rotor on an induction machine," *IEEE Trans. Ind. Appl.*, Vol. 28, No. 1, 165–171, Jan./Feb. 1992.
6. Bellini, A., F. Filippetti, G. Franceschini, C. Tassoni, and G. B. Kliman, "Quantitative evaluation of induction motor broken bars by means of electrical signature analysis," *IEEE Trans. Ind. Appl.*, Vol. 37, No. 5, 1248–1255, Sep./Oct. 2001.
7. Garcia-Perez, A., R. J. Romero-Troncoso, E. Cabal-Yepez,

R. A. Osornio-Rios, J. de Jesus Rangel-Magdaleno, and H. Miranda, "Startup current analysis of incipient broken rotor bar in induction motors using high-resolution spectral analysis," *Proc. of IEEE Int. Symposium on Diagnostics for Electric Machines, Power Electronics & Drives*, 657–663, Sept. 2011.

8. Kechida, R. and A. Menacer, "DWT wavelet transform for the rotor bars faults detection in induction motor," *Proc. of 2nd Int. Conf. on Electric Power and Energy Conversion Systems,* 1–5, Nov. 2011.
9. Keskes, H., A. Braham, and Z. Lachiri, "Broken rotor bar diagnosis in induction machines through Stationary Wavelet Packet Transform under lower sampling rate," *Proc. of 1st Int. Conf. on Renewable Energies and Vehicular Technology,* 452–459, Mar. 2012.
10. Riera-Guasp, M., J. A. Antonino-Daviu, M. Pineda-Sanchez, R. Puche-Panadero, and J. Perez-Cruz, "A general approach for the transient detection of slip-dependent fault components based on the discrete wavelet transform," *IEEE Trans. Ind. Electron.*, Vol. 55, No. 12, 4167–4180, Dec. 2008.
11. Douglas, H., P. Pillay, and A. K. Ziarani, "A new algorithm for transient motor current signature analysis using wavelets," *IEEE Trans. Ind. Appl.*, Vol. 40, No. 5, 1361–1368, Sep./Oct. 2004.
12. Faiz, J. and B.-M. Ebrahimi, "A new pattern for detecting broken rotor bars in induction motors during start-up," *IEEE Trans. Magn.*, Vol. 44, No. 12, 4673–4683, Dec. 2008.
13. Zhang, Z., Z. Ren, and W. Huang, "A novel detection method of motor broken rotor bars based on wavelet ridge," *IEEE Trans. Energy Convers.*, Vol. 18, No. 5, 417–423, Sept. 2003.
14. Ordaz-Moreno, A., R. de Jesus Romero-Troncoso, J. A. Vite-Frias, J. R. Rivera-Gillen, and A. Garcia-Perez, "Automatic online diagnosis algorithm for broken-bar detection on induction motors based on discrete wavelet transform for FPGA implementation," *IEEE Trans. Ind. Electron.*, Vol. 55, No. 5, 2193–2202, May 2008.
15. Pineda-Sanchez, M., M. Riera-Guasp, J. A. Antonino-Daviu, J. Roger-Folch, J. Perez-Cruz, and R. Puche-Panadero, "Instantaneous frequency of the left sideband harmonic during the start-up transient a new method for diagnosis of broken bars," *IEEE Trans. Ind. Electron.*, Vol. 56, No. 11, 4557–4570, Nov. 2009.
16. Supangat, R., N. Ertugrul, W. L. Soong, D. A. Gray, C. Hansen, and J. Grieger, "Broken rotor bar fault detection in induction motors using starting current analysis," *Proc. of European Conf. on Power Electronics and Applications*, 1–10, 2005.

17. Deleroi, W., "Squirrel cage motor with broken bar in the rotor — Physical phenomena and their experimental assessment," *Proc. of Int. Conf. on Electrical Machines*, 767–770, 1982.
18. Riera-Guasp, M., J. A. Antonino-Daviu, J. Roger-Folch, and M. P. Molina Palomares, "The use of the wavelet approximation signal as a tool for the diagnosis of rotor bar failures," *IEEE Trans. Ind. Appl.*, Vol. 44, No. 3, 716–726, May/Jun. 2008.
19. Sprooten, J., J. Gyselinck, and J. C. Maun, "Local and global effect of a broken bar in induction machines using fundamental electromagnetic laws and finite element simulations," *Proc. of IEEE Int. Symposium on Diagnostics for Electric Machines, Power Electronics & Drives*, 1–6, Sept. 2005.
20. Aroui, T., Y. Koubaa, and A. Toumi, "Magnetic coupled circuits modeling of induction machines oriented to diagnostics," *Leonardo Journal of Sciences*, Vol. 7, No. 13, 103–121, Jul./Dec. 2008.
21. Sprooten, J., J. Gyselinck, and J.-C. Maun, "Comparison of models of faulty induction motors: Performances and applications," *Proc. of IEEE Int. Symposium on Diagnostics for Electric Machines, Power Electronics & Drives*, 132–137, Sept. 2007.
22. Zhang, L. and T. S. Cheang, "Two new approaches to analysis of inner-fault of squirrel-cage rotor for three-phase induction motors," *Proc. of 5th Int. Conf. on Electrical Machines and Systems*, Vol. 1, 51–55, 2001.
23. Samonig, M. A., P. Nussbaumer, G. Stojicic, and T. M. Wolbank, "Analysis of rotor fault detection in inverter fed induction machines at no load by means of finite element method," *Proc. of 37th Annual Conf. on IEEE Ind. Electron. Society*, 1758–1763, Nov. 2011.
24. Zouzou, S. E., S. Khelif, N. Halem, and M. Sahraoui, "Analysis of induction motor with broken rotor bars using finite element method," *Proc. of 2nd Int. Conf. on Electric Power and Energy Conversion Systems*, 1–5, Nov. 2011.
25. Kuptsov, V. V., A. S. Sarvarov, and A. S. Gorzunov, "Development of current signature analysis technique to detect faults in induction motors by oscillograms of unsteady-state machine operation," *Vestnik Yuzhno-Ural'skogo Gosudarstvennogo Universiteta, Seriya Energetika,* Vol. 34, No. 12, 60–67, Jun. 2009 (in Russian).
26. Faiz, J., B. M. Ebrahimi, and M. B. B. Sharifian, "Time stepping finite element analysis of broken bars fault in a three-phase squirrel-cage induction motor," *Progress In Electromagnetics Research*, Vol. 68, 53–70, 2007.

27. Vaseghi, B., N. Takorabet, and F. Meibody-Tabar, "Transient finite element analysis of induction machines with stator winding turn fault," *Progress In Electromagnetics Research*, Vol. 95, 1–18, 2009.
28. Bouzida, A., O. Touhami, R. Ibtiouen, A. Belouchrani, M. Fadel, and A. Rezzoug, "Fault diagnosis in industrial induction machines through discrete wavelet transform," *IEEE Trans. Ind. Electron.*, Vol. 58, No. 9, 4385–4395, Sept. 2011.
29. Akın, B., S. Choi, U. Orguner, and H. A. Toliyat, "A simple real-time fault signature monitoring tool for motor drive embedded fault diagnosis systems," *IEEE Trans. Ind. Electron.*, Vol. 58, No. 5, 1990–2001, May 2011.
30. Cruz, S. M. A. and A. J. Marques Cardoso, "Stator winding fault diagnosis in three-phase synchronous and asynchronous motors, by the extended Park's vector approach," *IEEE Trans. Ind. Appl.*, Vol. 37, No. 5, 1227–1233, Sept./Oct. 2001.
31. Daubechies, I., "The wavelet transform, time-frequency localization and signal analysis," *IEEE Trans. Information Theory*, Vol. 36, No. 5, 961–1005, Sep. 1990.
32. Mallat, S., *A Wavelet Tour of Signal Processing*, Academic, San Diego, CA, 1999.
33. Misiti, M., Y. Misiti, G. Oppenheim, and J. M. Poggi, *Wavelet Toolbox, User's Guide for Matlab*, MathWorks, Natick, MA, Jun. 2004.
34. Abu-Rub, H., A. Iqbal, S. K. M. Ahmed, J. Guzinski, M. Adamowicz, and M. Rahiminia, "Rotor broken bar diagnostics in induction motor drive using Wavelet packet transform and ANFIS classification," *Proc. of Int. Conf. on Electric Machines & Drives Conference*, 365–370, May 2011.
35. Cusido, J., L. Romeral, J. A. Ortega, J. A. Rosero, and A. Garcia Espinosa, "Fault detection in induction machines using power spectral density in wavelet decomposition," *IEEE Trans. Ind. Electron.*, Vol. 55, No. 2, 633–643, Feb. 2008.
36. Sadeghian, A., Z. Ye, and B. Wu, "Online detection of broken rotor bars in induction motors by wavelet packet decomposition and artificial neural networks," *IEEE Trans. Instrum. Meas.*, Vol. 58, No. 7, 2253–2263, Jul. 2009.